Journal of Solid State Chemistry **161,** 233–242 (2001)
doi:10.1006/jssc.2001.9304, available online at http://www.idealibrary.com on IDEAL®

Novel Compounds $Sn_{10}In_{14}P_{22}I_8$ and $Sn_{14}In_{10}P_{21.2}I_8$ with Clathrate I Structure: Synthesis and Crystal and Electronic Structure

Mikhail M. Shatruk,* Kirill A. Kovnir,* Martin Lindsjö,‡ Igor A. Presniakov,†
Lars A. Kloo,‡ and Andrei V. Shevelkov*,[1]

*Inorganic Synthesis Laboratory, and †Chair of Radiochemistry, Department of Chemistry, Moscow State University, 119899 Moscow, Russia; and ‡Inorganic Chemistry, Department of Chemistry, The Royal Institute of Technology, S-100 44 Stockholm, Sweden

Received March 6, 2001; in revised form June 19, 2001; accepted July 12, 2001

Two new supramolecular pnictidehalides $Sn_{10}In_{14}P_{22}I_8$ (I) and $Sn_{14}In_{10}P_{21.2}I_8$ (II) have been synthesized using a standard ampoule technique. Both compounds possess the clathrate I type of structure. I crystallizes in the cubic space group $Pm\bar{3}n$ (No. 223) with the unit cell parameter $a = 11.0450(7)$ Å ($Z = 1$) while II reveals a complicated superstructure (space group $P4_2/m$ (No. 84), $a = 24.745(3)$ Å, $c = 11.067(1)$ Å, $Z = 5$) resulting from the partial ordering of vacancies at phosphorus sites. The crystal structures have been solved based on single-crystal X-ray diffraction data sets ($\omega - 2\theta$ scans, least-squares refinement against F^2) to $R = 0.0376$ ($Sn_{10}In_{14}P_{22}I_8$) and $R = 0.0569$ ($Sn_{14}In_{10}P_{21.2}I_8$). In both structures metal and phosphorus atoms form a cationic clathrate I framework hosting iodine atoms in the cavities. The composition of both phases complies with the Zintl–Klemm formalism which justifies the existence of vacancies in the structure of II. The ^{119}Sn Mössbauer spectroscopy data together with the results of the band structure calculations suggest that the electron density on tin atoms is reduced in favor of bands, which lie just below the Fermi level and must define electronic properties of the compounds in question. The differences in the crystal and electronic structures of the cationic tin clathrates are discussed. © 2001 Academic Press

INTRODUCTION

Up to date, a range of A_8E_{46} phases composed of an alkali metal A and a Group 14 element E is known (1–4). They all belong to a clathrate I structure type (5). Two different groups can be distinguished among these phases. The first one comprises compounds obeying the Zintl–Klemm concept (6) for valent compounds. As has been shown by Zhao and Corbett (4), the Zintl–Klemm formalism is satisfied due to the formation of vacancies in the host substructure ($A_8E_{44}\square_2$). Such structures are typical of germanides and stannides (4, 7, 8). The second group lies beyond the scope of the Zintl–Klemm formalism, and the compounds involved are characterized by the vacancy free structures. This type of structure is exhibited by silicides (8–10). Recently, it has been shown (10) that filling the vacancies allows such an interesting physical property as superconductivity to be achieved.

There exist a number of clathrate I type compounds characterized by the inverted host–guest polarity. In contrast to the above-mentioned tetrelides, they all obey the Zintl–Klemm formalism and no exceptions have been found so far. Von Schnering and Menke (11) were the first to report these kinds of compounds, $Ge_{38}Z_8X_8$ (Z = P, As, Sb; X = Cl, Br, I), which do not contain any vacancies. Recently, we showed that for such cationic clathrates it is also possible to have vacancies formed in the host substructure: the compound $Sn_{24}P_{19.3}I_8$ (12) contains a partially vacant phosphorus site in the covalent tin–phosphorus framework. To fill the vacancies, the lowering of the valence electron number utilized by the covalent framework of tin atoms is necessary. This may be achieved by substituting metal atoms with a lower number of valence electrons for tin atoms. The limit for such a substitution can be predicted using the Zintl–Klemm formalism and corresponds to the situation when all framework atoms possess a closed eight-electron shell.

The renewed interest in semiconducting clathrates is inspired by their promising thermoelectric properties, which make them good candidates for the thermoelectric cooling applications (13). In light of the promising properties, the search for new clathrates as well as the knowledge of the peculiarities of their crystal and electronic structures are of special interest (14, 15). In this work we describe synthesis of indium-containing compounds $Sn_{10}In_{14}P_{22}I_8$ and $Sn_{14}In_{10}P_{21.2}I_8$ and their crystal structures. The two compounds differ by the Sn/In ratio; besides, the former shows no vacancies in the metal–phosphorus framework.

[1]To whom the correspondence should be addressed. Dr. Andrei V. Shevelkov, Inorganic Synthesis Laboratory, Department of Chemistry, Moscow State University, Leninskie Gory, Moscow 119899, Russia. E-mail: shev@inorg.chem.msu.ru. Fax: (7-095)-939-4778.

0022-4596/01 $35.00
Copyright © 2001 by Academic Press
All rights of reproduction in any form reserved.

Electronic structures of the tin-based clathrates, which were assessed by means of Mössbauer spectroscopy and band structure calculations, are also discussed in comparison with the properties of the ternary phase $Sn_{24}P_{19.3}I_8$ (12).

EXPERIMENTAL

Samples. Metallic tin and indium (> 99.99% purity) were used as received. Red phosphorus was purified by washing consecutively with 30% aqueous solution of KOH, water, ethanol, and diethyl ether (twice) and then vacuum-dried. Tin(IV) iodide was synthesized by the reaction of excess tin with iodine in CCl_4 according to Ref. (16).

$Sn_{10}In_{14}P_{22}I_8$ and $Sn_{14}In_{10}P_{21.2}I_8$ were prepared by heating the respective stoichiometric mixtures of tin, indium, red phosphorus, and tin(IV) iodide in sealed silica tubes under vacuum at 773 K for 5 days. The samples were then reground and heated in sealed silica tubes under vacuum at 573 K for another 14 days, followed by slow cooling (about 20 K/h) to room temperature. After the second annealing the samples appeared as black air-stable homogenous powders. An X-ray analysis (Nonius FR-552 chamber, Cu$K\alpha_1$ radiation) showed no traces of starting materials. All reflections for the $Sn_{10}In_{14}P_{22}I_8$ sample were indexed in the cubic system with the unit cell parameter $a = 11.053(1)$ Å. The same subcell was found for the $Sn_{14}In_{10}P_{21.2}I_8$ sample; however, the indexing of all reflections was achieved only by enlarging the unit cell parameter by a factor of $(5)^{1/2}$ along the x and y axes, which thus led to a tetragonal unit cell with the parameters $a = 24.701(3)$ Å and $c = 11.044(2)$ Å.

Single-crystal X-ray diffraction. Suitable single crystals of $Sn_{10}In_{14}P_{22}I_8$ and $Sn_{14}In_{10}P_{21.2}I_8$ selected from the respective reaction products were mounted on a goniometer head of a CAD-4 (Nonius) diffractometer. In both cases the unit cell parameters refined based on 24 well-centered reflections in the angular range of $14^\circ < \theta < 16^\circ$ were in good agreement with those found from Guinier data. Data were recorded at room temperature with the data collection parameters listed in Table 1 and corrected for polarization and Lorentz effects. In the case of $Sn_{14}In_{10}P_{21.2}I_8$, a semiempirical absorption correction was applied to the data based on azimuthal scans of six reflections having χ angles close to 90°. For $Sn_{10}In_{14}P_{22}I_8$, an analytical absorption correction was applied to the data based on the actual shape of the crystal.

Crystal structure refinement. The crystal structure of $Sn_{10}In_{14}P_{22}I_8$ was solved in the space group $Pm\bar{3}n$ by direct methods (SHELXS-86 (17)), which revealed all atomic positions. The analysis of the difference Fourier map showed the absence of any chemically meaningful peaks near all atomic positions, including, being the most important, the only metal site. Thus, the existence of the unique 24-fold site for the metal atoms was confirmed. It was not possible to distinguish between tin and indium atoms in this position. Based on the synthesis of the monophase sample, the mixed occupancies of the metal site were taken as fixed values corresponding to 42% Sn and 58% In. The refinement of occupancy factors for the phosphorus and iodine atoms did not reveal any substantial deviation of the values from unity. Final refinement against F^2 (SHELXL-93 (18)) with the anisotropic thermal displacement parameters of all atoms led to $R = 0.0376$ and the atomic parameters listed in Table 2. Selected interatomic distances and bond angles are given in Table 3.

Systematic absences indicated two possible space groups in the case of $Sn_{14}In_{10}P_{21.2}I_8$, $P4_2$ and $P4_2/m$. The structure was solved in the centrosymmetric $P4_2/m$ space group. The application of direct methods [SHELXS-86 (17)] allowed us to localize 8 atomic positions of the iodine atoms and 15 atomic positions of the metal atoms. The rest of the atoms (2 I, 5 metal, and 17 P) were assigned on the basis of the

TABLE 1
Data Collection and Structure Refinement Parameters for $Sn_{14}In_{10}P_{21.2}I_8$ and $Sn_{10}In_{14}P_{22}I_8$

Formula	$Sn_{10}In_{14}P_{22}I_8$	$Sn_{14}In_{10}P_{21.2}I_8$
Space group	$Pm\bar{3}n$ (No. 223)	$P4_2/m$ (No. 84)
Unit cell dimensions, Å	$a = 11.0450(7)$	$a = 24.745(3)$
		$c = 11.067(1)$
V, Å^3	1347.4(2)	6776.5(13)
Z	1	5
ρ_{calc}, Mg/m^3	5.535	5.521
λ, Å	0.71069	0.71069
μ, mm^{-1}	15.643	15.670
Scanning mode	ω–2θ	ω–2θ
θ range for data collection, deg	2.61 to 27.93	2.02 to 24.98
Refl. collected	1711	6589
Independent refl.	320 [R(int) = 0.0475]	6271 [R(int) = 0.0620]
Data/parameters	320/16	6271/269
Extinction coeff.	0.00026(9)	—
R [$F_o > 2\sigma(F_o)$]	$R_1 = 0.0376$, $wR_2 = 0.0500$	$R_1 = 0.0569$, $wR_2 = 0.1344$
G-o-f on F^2	1.479	1.056
Largest diff. peak and hole, e Å^{-3}	0.834 and −0.668	3.701 and −2.550

TABLE 2
Atomic Parameters for $Sn_{10}In_{14}P_{22}I_8$

Atom	Site	x/a	y/b	z/c	s.o.f.	U(eq)
I(1)	2a	0	0	0	1	0.0115(3)
I(2)	6d	$\frac{1}{4}$	0	$\frac{1}{2}$	1	0.0183(2)
M^a	24k	0.3097(4)	0	0.1252(5)		0.0142(2)
P(1)	16	0.1928(1)	0.1928	0.1928	1	0.0107(7)
P(2)	6c	$\frac{1}{2}$	0	$\frac{1}{4}$	1	0.0088(4)

[a] M = 42% Sn and 58% In.

TABLE 3
Selected Interatomic Distances (Å) and Bond Angles (°) in the Structure of $Sn_{10}In_{14}P_{22}I_8$

Interatomic distances		Bond angles	
P(1)–P(1)	2.190(4)	P(1)–P(1)–*M*	110.60(4)
P(1)–*M*[a]	2.600(1) (×3)	*M*–P(1)–*M*	108.32(4)
P(2)–*M*	2.514(1) (×4)	*M*–P(2)–*M*	107.5(1)
		M–P(2)–*M*	113.49(2)
M–*M*	2.766(1)		
M–P(1)	2.600(1) (×2)	P(1)–*M*–P(2)	104.95(4)
M–P(2)	2.514(1)	P(1)–*M*–P(1)	109.97(5)
		P(2)–*M*–*M*	123.26(1)
		P(1)–*M*–*M*	106.68(2)

[a]The mixed Sn/In metal site is designated as *M*.

difference Fourier map. Based on their coordination, the P atoms were divided into two types: atoms that form one P–P bond (type *A*) and those without such a bond (type *B*). The isotropic thermal parameter was set equal for all atoms of the same sort, while occupancy factors for all phosphorus sites were unconstrained. The refinement showed that the occupancy factors for the type *A* P atoms did not deviate substantially from unity. The same situation was observed for all but two type *B* atoms. The occupancy factors for atoms P(2) and P(4) were both about 0.5. However, the respective e.s.d.'s were of the same order of magnitude as the values themselves because of the poor quality of the data (low intensities which did not allow us to acquire data beyond $\theta = 25°$). Therefore, the occupancy factors for these two atoms were frozen at 0.5, while those for all other phosphorus atoms were constrained to unity. Final refinement against F^2 [SHELXL-93 (18)] using anisotropic thermal displacement parameters for iodine and tin atoms and isotropic ones for phosphorus atoms led to $R = 0.0569$. The atomic parameters are listed in Table 4, and important interatomic distances and bond angles are summarized in Table 5.

Mössbauer spectroscopy. The ^{119}Sn spectra were recorded using a conventional constant acceleration Mössbauer spectrometer. Measurements were performed over the temperature range of 80–300 K with the $Ca^{119m}SnO_3$ source maintained at room temperature. Isomer chemical shifts are referenced to a $CaSnO_3$ absorber at 300 K. The samples of $Sn_{10}In_{14}P_{22}I_8$ and $Sn_{14}In_{10}P_{21.2}I_8$ were checked for monophasity by means of the profile analysis of the respective X-ray diffractograms (STADI-P (STOE), Cu$K\alpha_1$ radiation).

Calculations. The band structure calculations were performed using the CRYSTAL98 program package (19). All calculations included a converged SCF run and evaluation of band structure and Density of States, at both Hartree–Fock, density functional theory (SVWN) and hybrid density functional theory level (B3LYP). Hay and Wadt Large-Core (HAYWLC) pseudopotentials were applied as implemented in CRYSTAL98 to all atom types, and valence basis sets by Hay and Wadt, with double-zeta quality, was used (20). However, the most diffuse functions of the metals were removed to minimize convergence problems.

TABLE 4
Atomic Parameters for $Sn_{14}In_{10}P_{21.2}I_8$

Atom	Site	*x*/*a*	*y*/*b*	*z*/*c*	s.o.f.	*U* (iso/eq)[a]
I(1)	2*a*	½	0	0	1	0.011(1)
I(2)	2*e*	0	0	¼	1	0.011(1)
I(3)	4*j*	0.8007(2)	0.0997(1)	½	1	0.0127(7)
I(4)	4*j*	0.4003(2)	0.2997(2)	½	1	0.0101(7)
I(5)	4*j*	0.4485(2)	0.3993(2)	0	1	0.023(1)
I(6)	4*j*	0.3990(2)	0.0503(2)	½	1	0.027(1)
I(7)	4*j*	0.8011(2)	0.3494(2)	½	1	0.0178(9)
I(8)	4*j*	0.2502(2)	−0.0008(2)	0	1	0.0117(8)
I(9)	4*j*	0.1922(2)	0.1495(2)	½	1	0.0150(9)
I(10)	8*k*	0.6013(2)	0.2004(1)	0.2493(3)	1	0.0211(5)
M(1)	4*j*	0.0870(2)	0.0525(2)	0	1	0.0134(9)
M(2)	4*j*	0.5886(2)	0.3000(2)	0	1	0.010(1)
M(3)	4*j*	0.5501(2)	0.2868(2)	½	1	0.014(1)
M(4)	4*j*	0.7008(2)	0.2113(2)	½	1	0.018(1)
M(5)	4*j*	0.6886(2)	0.2511(2)	0	1	0.019(1)
M(6)	4*j*	0.4981(2)	0.1880(2)	½	1	0.017(1)
M(7)	4*j*	0.1008(2)	0.0126(2)	½	1	0.019(1)
M(8)	4*j*	0.6510(2)	0.1107(2)	½	1	0.0136(9)
M(9)	4*j*	0.5111(2)	0.1506(2)	0	1	0.020(1)
M(10)	4*j*	0.6129(2)	0.0984(2)	0	1	0.019(1)
M(11)	8*k*	0.0494(1)	0.4762(2)	0.1906(3)	1	0.0188(8)
M(12)	8*k*	0.8511(1)	0.0745(1)	0.1901(3)	1	0.0167(6)
M(13)	8*k*	0.3502(1)	0.3247(1)	0.1899(3)	1	0.0139(7)
M(14)	8*k*	0.3378(1)	0.1758(1)	0.3794(3)	1	0.0159(7)
M(15)	8*k*	0.3758(1)	0.0617(1)	0.1266(3)	1	0.0136(7)
M(16)	8*k*	0.2614(1)	0.0237(1)	0.3759(3)	1	0.0180(7)
M(17)	8*k*	0.4623(1)	0.4239(2)	0.3740(3)	1	0.0175(7)
M(18)	8*k*	0.2244(1)	0.1372(1)	0.1272(3)	1	0.0179(7)
M(19)	8*k*	0.4495(1)	0.2746(1)	0.1891(3)	1	0.0133(6)
M(20)	8*k*	0.7500(1)	0.1253(1)	0.1905(3)	1	0.0162(7)
P(1)	2*f*	½	½	¼	1	0.002(4)
P(2)	4*j*	0.5513(1)	0.1018(1)	½	0.5	0.000(5)
P(3)	4*j*	0.4978(5)	0.2551(5)	0	1	0.000(3)
P(4)	4*j*	0.6481(1)	0.2961(1)	½	0.5	0.000(5)
P(5)	4*j*	0.7005(5)	0.1496(5)	0	1	0.000(3)
P(6)	4*j*	0.1005(5)	−0.0442(5)	0	1	0.000(2)
P(7)	8*k*	0.2988(5)	0.0970(5)	0.2537(12)	1	0.013(2)
P(8)	8*k*	0.5174(4)	0.3386(4)	0.6979(10)	1	0.006(2)
P(9)	8*k*	0.2127(4)	0.2398(4)	0.1955(8)	1	0.000(2)
P(10)	8*k*	0.4381(4)	0.1807(4)	0.3035(10)	1	0.009(2)
P(11)	8*k*	0.6177(4)	0.0361(4)	0.1888(9)	1	0.006(2)
P(12)	8*k*	0.1613(4)	0.0153(3)	0.3127(10)	1	0.000(2)
P(13)	8*k*	0.5872(4)	0.3606(4)	0.1920(9)	1	0.006(2)
P(14)	8*k*	0.4590(4)	0.1132(5)	0.1943(10)	1	0.010(2)
P(15)	8*k*	0.2843(4)	0.2627(4)	0.3147(8)	1	0.004(2)
P(16)	8*k*	0.1395(4)	0.0883(4)	0.1938(9)	1	0.001(2)
P(17)	8*k*	0.6807(4)	0.0640(4)	0.6898(8)	1	0.000(2)

[a]All phosphorus atoms were refined isotropically.

TABLE 5
Selected Interatomic Distances (Å) in the Structure of $Sn_{14}In_{10}P_{21.2}I_8$

P(1)–*M*(17)	2.510(3) (×4)	P(11)–*M*(15)	2.52(1)
P(2)–*M*(6)	2.51(3)	P(12)–P(16)	2.30(1)
P(2)–*M*(8)	2.48(3)	P(12)–*M*(7)	2.56(1)
P(2)–*M*(11)	2.57(2) (×2)	P(12)–*M*(12)	2.622(9)
P(3)–*M*(2)	2.51(1)	P(12)–*M*(16)	2.58(1)
P(3)–*M*(9)	2.61(1)	P(13)–*M*(2)	2.60(1)
P(3)–*M*(19)	2.457(7) (×2)	P(13)–*M*(13)	2.55(1)
P(4)–*M*(3)	2.44(3)	P(13)–*M*(17)	2.63(1)
P(4)–*M*(4)	2.47(3)	P(14)–*M*(9)	2.67(1)
P(4)–*M*(13)	2.58(2) (×2)	P(14)–*M*(11)	2.59(1)
P(5)–*M*(5)	2.53(1)	P(14)–*M*(15)	2.54(1)
P(5)–*M*(10)	2.51(1)	P(15)–*M*(5)	2.52(1)
P(5)–*M*(20)	2.512(7) (×2)	P(15)–*M*(13)	2.63(1)
P(6)–*M*(1)	2.42(1)	P(15)–*M*(14)	2.62(1)
P(6)–*M*(7)	2.59(1)	P(16)–*M*(1)	2.66(1)
P(6)–*M*(12)	2.535(8) (×2)	P(16)–*M*(12)	2.55(1)
P(7)–*M*(14)	2.58(1)	P(16)–*M*(18)	2.53(1)
P(7)–*M*(15)	2.53(1)	P(17)–*M*(8)	2.507(9)
P(7)–*M*(16)	2.44(1)	P(17)–*M*(16)	2.70(1)
P(7)–*M*(18)	2.52(1)	P(17)–*M*(20)	2.65(1)
P(8)–P(13)	2.18(1)		
P(8)–*M*(3)	2.66(1)	*M*(1)–*M*(7)	2.737(7)
P(8)–*M*(17)	2.64(1)	*M*(2)–*M*(5)	2.754(7)
P(8)–*M*(19)	2.63(1)	*M*(3)–*M*(6)	2.761(6)
P(9)–P(15)	2.28(1)	*M*(4)–*M*(8)	2.777(6)
P(9)–*M*(4)	2.62(1)	*M*(5)–*M*(2)	2.754(7)
P(9)–*M*(18)	2.667(9)	*M*(9)–*M*(10)	2.832(7)
P(9)–*M*(20)	2.52(1)	*M*(11)–*M*(11)	2.714(6)
P(10)–P(14)	2.12(2)	*M*(12)–*M*(20)	2.798(4)
P(10)–*M*(6)	2.64(1)	*M*(13)–*M*(19)	2.753(4)
P(10)–*M*(14)	2.62(1)	*M*(14)–*M*(14)	2.669(6)
P(10)–*M*(19)	2.66(1)	*M*(15)–*M*(15)	2.803(7)
P(11)–P(17)	2.17(1)	*M*(16)–*M*(16)	2.746(7)
P(11)–*M*(10)	2.60(1)	*M*(17)–*M*(17)	2.788(6)
P(11)–*M*(11)	2.70(1)	*M*(18)–*M*(18)	2.816(7)

Note. Ranges for the valence angles (°): *M*–P–M, 103.7(4) to 116.8(5); P–P–*M*, 105.9(5) to 117.0(5); P–*M*–P, 102.5(4) to 127.7(3); P–*M*–*M*, 104.0(3) to 125.3(5).

RESULTS AND DISCUSSION

In the crystal structure of $Sn_{10}In_{14}P_{22}I_8$ (Fig. 1), tin, indium and phosphorus atoms form a three-dimensional framework hosting iodine atoms in its cavities. The metal atom is tetrahedrally coordinated by 3 phosphorus (2.51–2.60 Å) and 1 metal (2.77 Å) atoms. Two crystallographically independent phosphorus atoms differ by their coordination: P(1) forms 3 P–*M* bonds (2.60 Å) and 1 P–P bond [2.19 Å, being characteristic of a single P–P bond (21)], while P(2) is surrounded by 4 metal atoms (2.51 Å). The iodine atoms occupy two large cavities: I(1) appears in a dodecahedron comprised of 20 framework atoms, while I(2) is found in a tetrakaidecahedron which includes 24 framework atoms. The distances between iodine and the framework atoms range from 3.69 to 4.19 Å depending on the type of the iodine atom.

The $Sn_{10}In_{14}P_{22}I_8$ formula corresponds to the ideal clathrate I composition: for the 8 iodine atoms there are 46 framework atoms which completely occupy the 24*k*, 16*i* and 6*c* sites. The latter position is partially occupied in the structure of $Sn_{24}P_{19.3}I_8$ (12), and this is interrelated with the distribution of tin atoms among two partially occupied 24-fold sites. Filling the vacancies in the phosphorus site might remove the splitting of the metal position, observed in the case of the $Sn_{10}In_{14}P_{22}I_8$ structure with the fully occupied 24*k* metal site.

The crystal structure of $Sn_{14}In_{10}P_{21.2}I_8$ is the first established superstructure of the clathrate I type (Fig. 2). The clathrate I motif is preserved despite the enlarged unit cell derived from the cubic clathrate I cell by multiplying the *a* value by a factor of $(5)^{1/2}$ in two directions, hence, enlarging the unit cell volume five times. This complicated tetragonal superstructure arises due to the partial ordering of vacancies in phosphorus sites. The structure of $Sn_{14}In_{10}P_{21.2}I_8$ is therefore analogous to the $Sn_{24}P_{19.3}I_8$ structure. Not only are these structures characterized by partial occupancies of some phosphorus sites, but they also resemble each other in having both four- and three-coordinated metal atoms. However, the splitting of the unique metal site is evidently present only in the former structure. The three-coordinated sites in $Sn_{14}In_{10}P_{21.2}I_8$ emerge because of the half-occupancy of the P(2) and P(4) sites (see Table 4). The structure of $Sn_{14}In_{10}P_{21.2}I_8$ contains 120 metal atoms per unit cell, of which 16 consequently are three-coordinated and all others are four-coordinated.

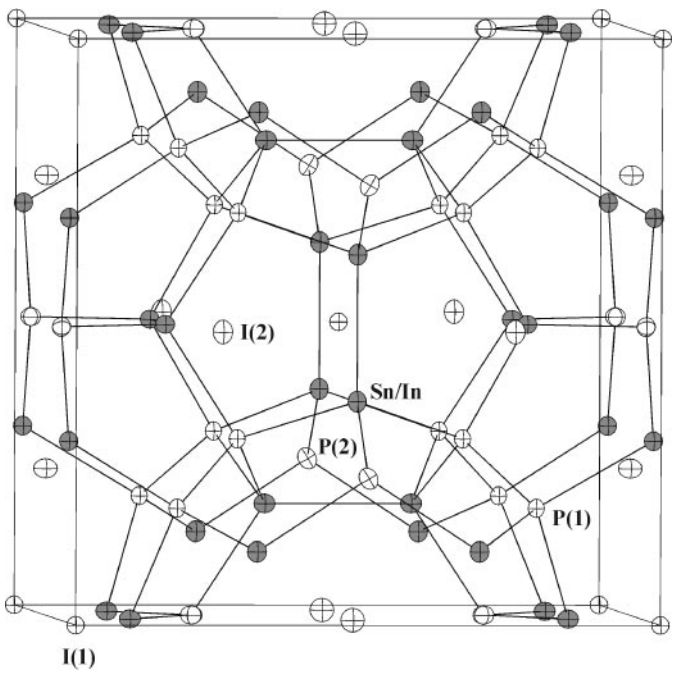

FIG. 1. A view of the crystal structure of $Sn_{10}In_{14}P_{22}I_8$ (50% probability ellipsoids).

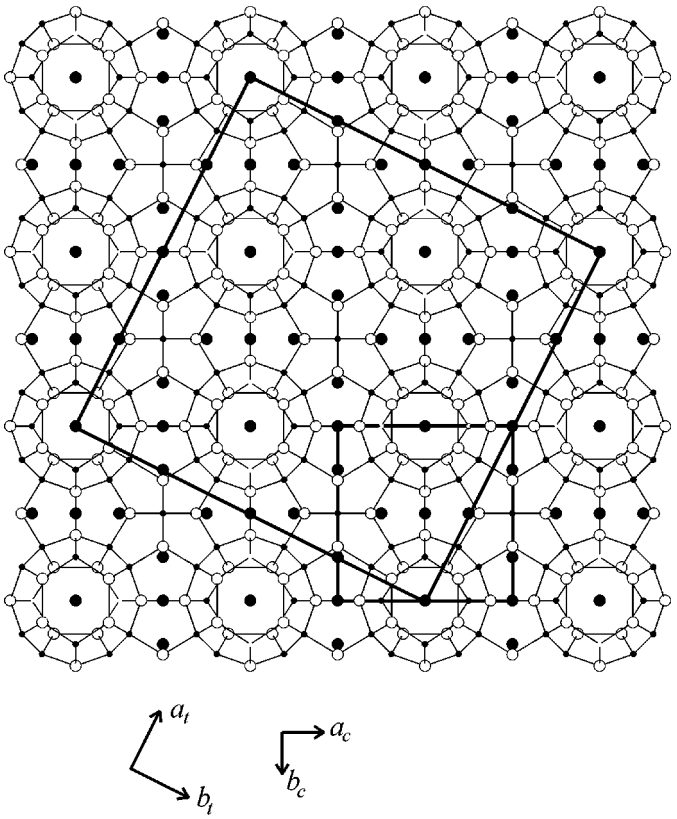

FIG. 2. A projection of the crystal structure of $Sn_{14}In_{10}P_{21.2}I_8$ on (001). Both the tetragonal cell and cubic subcell are shown with thick lines. Large filled circles, iodine; large open circles, metals; small filled circles, 100% occupied phosphorus sites; small open circles, 50% occupied phosphorus sites.

Therefore, a vacancy concentration of 13.33% in the phosphorus sites, which are not involved in P–P bonding, implies the same content of three-coordinated metal positions.

In the structure of $Sn_{24}P_{19.3}I_8$ (12) we also might have observed a superstructure resulting from the ordering of vacancies. However, the superstructure unit cell parameters are probably too large to be resolved by means of the X-ray single-crystal analysis. On the other hand, the $Sn_{14}In_{10}P_{21.2}I_8$ structure gives a striking example of vacancy ordering and also highlights a more subtle feature of the $Sn_{24}P_{19.3}I_8$ structure. There are two 24-fold tin sites in the latter, the occupancy factors being 0.45 for three-coordinated Sn(1) atoms and 0.55 for the four-coordinated Sn(2) atoms. Since each Sn(1) atom forms a Sn(1)–Sn(2) bond, the question immediately arises whether the coordination of all Sn(2) atoms is the same. Indeed, it is quite obvious that the Sn(1) sites are less occupied, and given the same point symmetry for both tin positions, we might appeal to the fact that there is an excess of Sn(2) atoms which do not form the Sn(1)–Sn(2) bonds. The problem is resolved if we imagine a superstructure where all tin atoms generally are four-coordinated by one Sn and three P atoms, but a certain part of them have one phosphorus neighbor missing due to the (partial) vacancy formation in the P sites. $Sn_{14}In_{10}P_{21.2}I_8$ represents an example of such a superstructure.

The compositions of both tin–indium pnictideiodides may be justified on the basis of the Zintl–Klemm formalism. It is shown in (12) that an ideal $Sn_{24}P_{19.2}I_8$ composition arises due to the removal of 2.8 atoms per unit cell from the 6*c* phosphorus site to compensate for $2.8 \times 5 = 14$ excessive electrons in the hypothetical vacancy-free $[Sn_{24}P_{22}]^{8+}$ framework. One way to fill the phosphorus site is to decrease the number of electrons given to the framework by the metal atoms. If we take a post-transition metal M with n valence electrons per atom, then the number of vacancies per unit cell in an $Sn_{24-x}M_xP_{22-\delta}I_8$ structure is

$$\delta = (14 - (4 - n) \cdot x)/5.$$

Thus, we can predict that for indium ($n = 3$) the vacancy-free composition is reached at $x = 14$, as we see is the case of $Sn_{10}In_{14}P_{22}I_8$. It could be argued that the structure was solved without distinguishing between Sn and In atoms. Nevertheless, the composition $Sn_{10}In_{14}P_{22}I_8$ was confirmed by the monophase product synthesis. Besides, the complete filling of phosphorus sites was unambiguously proven by the crystal structure refinement.

In the same way, we can calculate over other pairs of δ and x values. At $x = 10$, the δ value of 0.8 is obtained, which coincides with the composition of the phase-pure sample, $Sn_{14}In_{10}P_{21.2}I_8$. The value of $\delta > 0$ implies vacancy formation in the phosphorus substructure. Indeed, as has been shown by the crystal structure refinement, this compound exhibits the complicated tetragonal superstructure arising due to the ordering of vacancies in phosphorus sites. Consequently, as was described above, in the covalent framework of the $Sn_{14}In_{10}P_{21.2}I_8$ structure tin atoms with different coordination numbers occur. This fact and the ratio of three- to four-coordinated tin atoms were further proved by means of Mössbauer spectroscopy.

The parameters of ^{119}Sn Mössbauer spectra recorded from $Sn_{10}In_{14}P_{22}I_8$ and $Sn_{14}In_{10}P_{21.2}I_8$ are given in Table 6. The spectrum recorded from $Sn_{10}In_{14}P_{22}I_8$ shows one doublet in accordance with one unique tin site in the ideal clathrate I structure. The chemical isomer shift of $1.77\ mm\ s^{-1}$ is close to the value of $1.84\ mm\ s^{-1}$ recorded from the four-coordinated tin in the parent phase $Sn_{24}P_{19.3}I_8$ (12). A slight broadening of the resonance line ($\Gamma = 1.4\ mm\ s^{-1}$) can be attributed to a superposition of two doublets having very close values, reflecting two statistically probable types of tin coordination, 1Sn + 3P and 1In + 3P. The quadrupole splitting of $1.34\ mm\ s^{-1}$ is much larger than that found for the tetra-coordinated tin in $Sn_{24}P_{19.3}I_8$ ($0.72\ mm\ s^{-1}$). Such a difference in the quadrupole constants ($e^2qQ = 2\Delta$) can be explained by a different degree of distortion of tetrahedral coordination of tin. To

TABLE 6
The ^{119}Sn Mössbauer Parameters Recorded at 300 K

Compound	Site[a]	$\delta \pm 0.01$, mm/s	$\Delta \pm 0.01$, mm/s	$A \pm 1$, %	G^b
$Sn_{10}In_{14}P_{22}I_8$	Sn(I)	1.77	1.34	100	100
$Sn_{14}In_{10}P_{21.8}I_8$					
	Sn(I)	1.83	1.35	88	86.7
	Sn(II)	2.56	0.30	12	13.3

Note. Parameters do not deviate noticeably from those recorded at 80 K.
[a]Labeling: Sn(I), 4-coordinated tin; Sn(II), 3 + 3-coordinated tin.
[b]Occupancies from the crystal data.

TABLE 7
Calculated Orbital Occupancies (N_i), Asymmetry Parameter (η), and Quadrupole Splitting (Δ, in mm/s) According to the Tawnes–Dailey Model (see Eqs. [1]–[4])

Compound	N_z	N_x	N_y	η	$\Delta_{calc} \equiv eq^2Q/2$
$Sn_{24}P_{19.3}I_8$	$0.67 + 0.82\alpha^2$	$1.99\alpha^2$	$1.85\alpha^2$	0.48	0.72
$Sn_{10}In_{14}P_{22}I_8$[a]	$0.80 + 0.67\alpha^2$	$2.01\alpha^2$	$1.71\alpha^2$	0.73	1.15
$Sn_{10}In_{14}P_{22}I_8$[b]	$1.61\alpha_1^2 + 0.67\alpha_2^2$	$2.01\alpha^2$	$1.71\alpha^2$	0.39	1.36

[a]Assuming that tin is coordinated by 1Sn + 3P.
[b]Assuming that tin is coordinated by 1In + 3P.

assess a correlation between the local tin environment and quadrupole constants, we calculated the theoretical values of the constants in the frames of the Townes–Dailey model (22) according to the formula

$$e^2qQ = e^2qQ_0(N_z - \tfrac{1}{2}(N_x + N_y))(1 + \eta^2/3)^{1/2}, \quad [1]$$

where N_i is the occupancy of the corresponding orbital, $\eta = (N_x - N_y)/N_z$ is the asymmetry parameter, and $e^2qQ_0 = 6\ \mathrm{mm\,s^{-1}}$ is a quadrupole constant for a single p_z electron. The molecular wavefunction is expressed in the LCAO approximation as

$$\Psi_i = \alpha_i h_i + \beta_i \phi_L \quad (\alpha^2 + \beta^2 = 1), \quad [2]$$

where ϕ_L is a ligand orbital and h_i is a hybrid tin orbital. Each hybrid orbital has contributions of the atomic orbitals

$$h_i = C_s^i\phi_s + C_x^i\phi_x + C_y^i\phi_y + C_z^i\phi_z, \quad [3]$$

where ϕ_j is an atomic s or p orbital. The C_j^i coefficients provide a measure of participation of the jth atomic orbital in the h_i hybrid orbital. They depend only upon the geometry of the local environment of a given tin atom. Having evaluated the C_j^i-coefficients from the crystal structures of $Sn_{24}P_{19.3}I_8$ (12) and $Sn_{10}In_{14}P_{22}I_8$, we then calculated the occupancies, N_i, as

$$N_z = \sum 2\alpha_i^2(C_z^i)^2; \quad N_x = \sum 2\alpha_i^2(C_x^i)^2; \quad N_y = \sum 2\alpha_i^2(C_y^i)^2, \quad [4]$$

where α_i accounts for the Pauling electronegativity χ of the atoms bonded to tin. In our work we evaluated α using its dependence upon the difference in χ as $\alpha^2 = (1 - \frac{1}{2}(\Delta\chi))/2$. Thus, obtained N_i values were used in Eq. [1] to calculate the constants presented in Table 7.

The results obtained with the help of the Townes–Dailey model are in good agreement with the observed values. They confirm that the deviation from the ideal tetrahedral geometry leads to the imbalance of the p_z and $p_{x,y}$ tin electrons, resulting in different values of the quadrupole constants. Accordingly, the highest degree of the tetrahedron distortion in $Sn_{10}In_{14}P_{22}I_8$ leads to the largest quadrupole splitting of $1.34\ \mathrm{mm\,s^{-1}}$.

The ^{119}Sn Mössbauer spectrum recorded from $Sn_{14}In_{10}P_{21.2}I_8$ is best fitted to a superposition of two doublets (Fig. 3). Their parameters (Table 7) are quite differ-

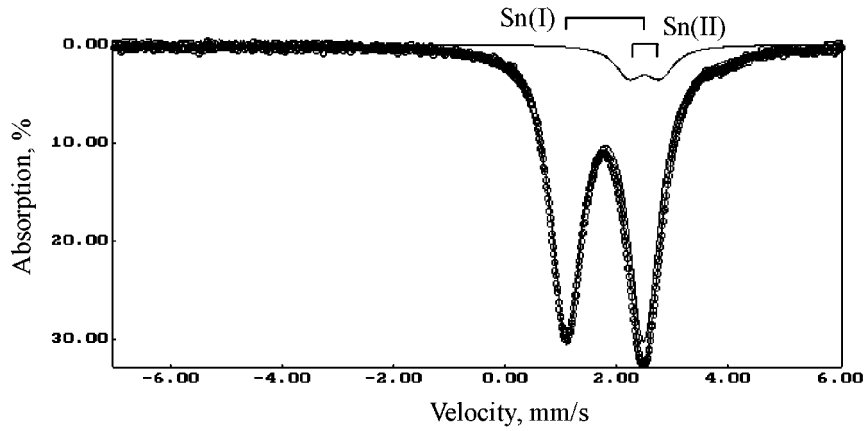

FIG. 3. The ^{119}Sn Mössbauer spectrum recorded from $Sn_{14}In_{10}P_{21.2}I_8$. (The Sn(I) and Sn(II) labels are the same as in Table 6.)

ent, reflecting the presence of two different kinds of tin atoms. The first doublet has parameters very close to those found for tin in $Sn_{10}In_{14}P_{22}I_8$ and can thus be assigned to tin atoms in a distorted tetrahedral environment. The parameters of the second doublet resemble those recorded from Sn_4P_3 for which the values of $\delta = 2.54$ and $\Delta = 0.46\,mm\,s^{-1}$ were obtained (23). There are two different tin sites in the layered structure of Sn_4P_3 (24). In both of them, tin forms three short (2.66–2.73 Å) bonds with phosphorus within the same layer and distant bonds with either three tin (3.25 Å) or three phosphorus (2.97 Å) atoms of the neighboring layer. In such a way a 3 + 3 pseudo-octahedral coordination of tin is achieved, which is similar to the coordination of one kind of tin atom in $Sn_{14}In_{10}P_{21.2}I_8$ and $Sn_{24}P_{19.3}I_8$. It should be noted that in these phases the related intensities of the signals from 4- and 3 + 3-coordinated atoms are in excellent agreement with the crystallographic occupancies of the respective sites.

The above-described 3 + 3 environment of the tin atoms suggests an sp^3-hybridized system with a lone pair pointing toward three distant neighbors. Despite the apparent localization of the lone pair, the quadrupole splitting is only 0.30 $mm\,s^{-1}$, indicating that the stereoactivity of the lone pair is substantially suppressed. [The quadrupole splitting is much lower than that found for numerous tin(II) compounds having a pronounced stereoactive lone pair (25)]. Since the

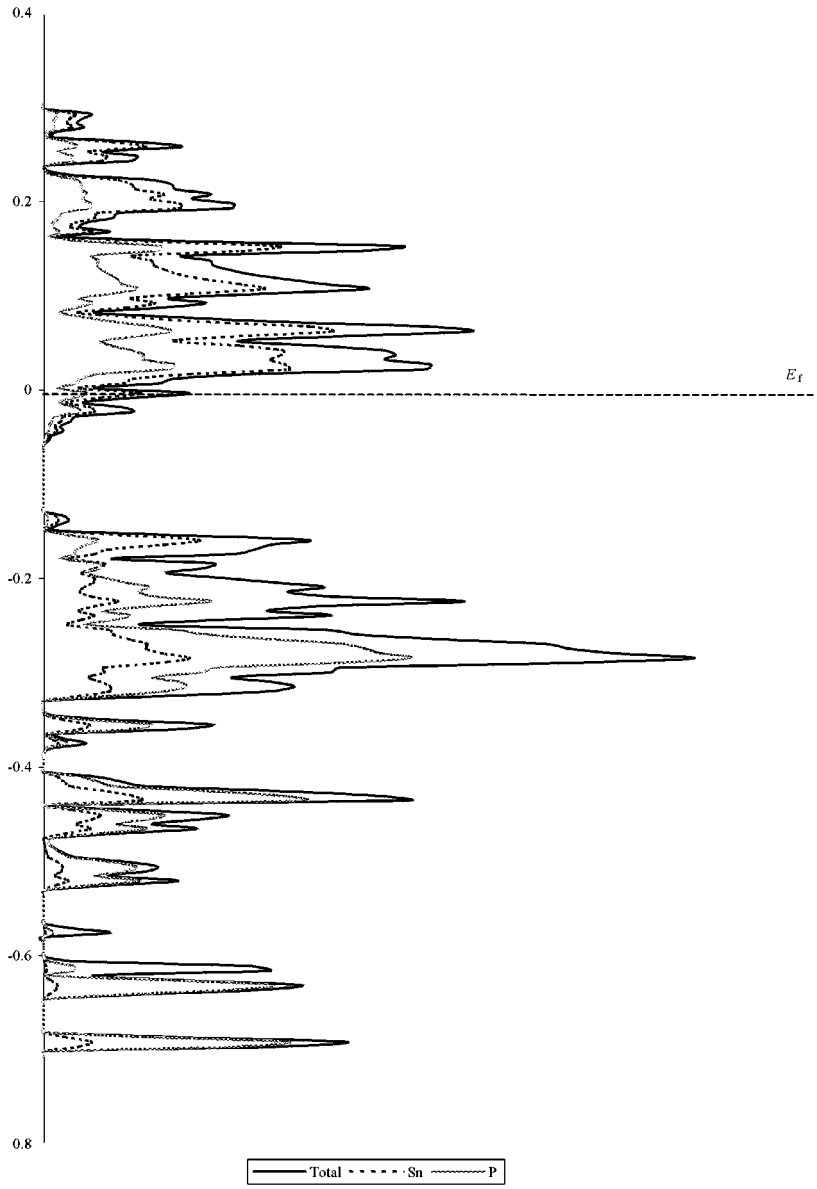

FIG. 4. The DOS for $Sn_{24}P_{22}I_8$, hybrid density functional level (B3LYP). $E_F = -0.005$ eV.

quadrupole splitting is proportional to the amount of the p character, the low value of $\Delta = 0.30\,\mathrm{mm\,s^{-1}}$ could be associated with a dominant contribution of the tin 5s electrons to the lone pair. Consequently, a much larger isomer chemical shift would be expected; the values of $\delta = 4.0\,\mathrm{mm\,s^{-1}}$ and higher were reported in the literature for tin(II) compounds with a suppressed lone pair (26). The observed isomer chemical shift, however, is only $2.60\,\mathrm{mm\,s^{-1}}$ (Table 6). We believe that involving the tin 5s electrons in the band structure, through interactions with the close and distant neighbors, reduces the charge density on the tin nucleus and thus decreases the isomer chemical shift.

The band structure calculations were performed on three compounds, $Sn_{24}P_{22}I_8$, $Sn_{10}In_{14}P_{22}I_8$, and $Sn_{24}P_{19}I_8$. The first object is a hypothetical clathrate constructed by filling all the framework positions in the space group $Pm\bar{3}n$. The second object is a real derivative achieved by a random distribution of 14 indium atoms among the 24 metal atom positions. The third object has an almost real composition which is only 0.3 P atoms per formula short (12). It is constructed in such a way that there are two types of Sn atoms, 4- and 3 + 3-coordinated, in equal numbers, compared to the observed 55:45 ratio.

The plots of density of states (DOS) are given in Figs. 4–6. It is clear from the drawings that $Sn_{24}P_{22}I_8$, if it existed, would be a metal. The other compounds should be semiconductors. We previously (12) observed the semiconducting dependence of conductivity on temperature for $Sn_{24}P_{19.3}I_8$ and estimated the gap width to 0.04 eV, being quite comparable to the calculated value of $\sim$0.01 eV.

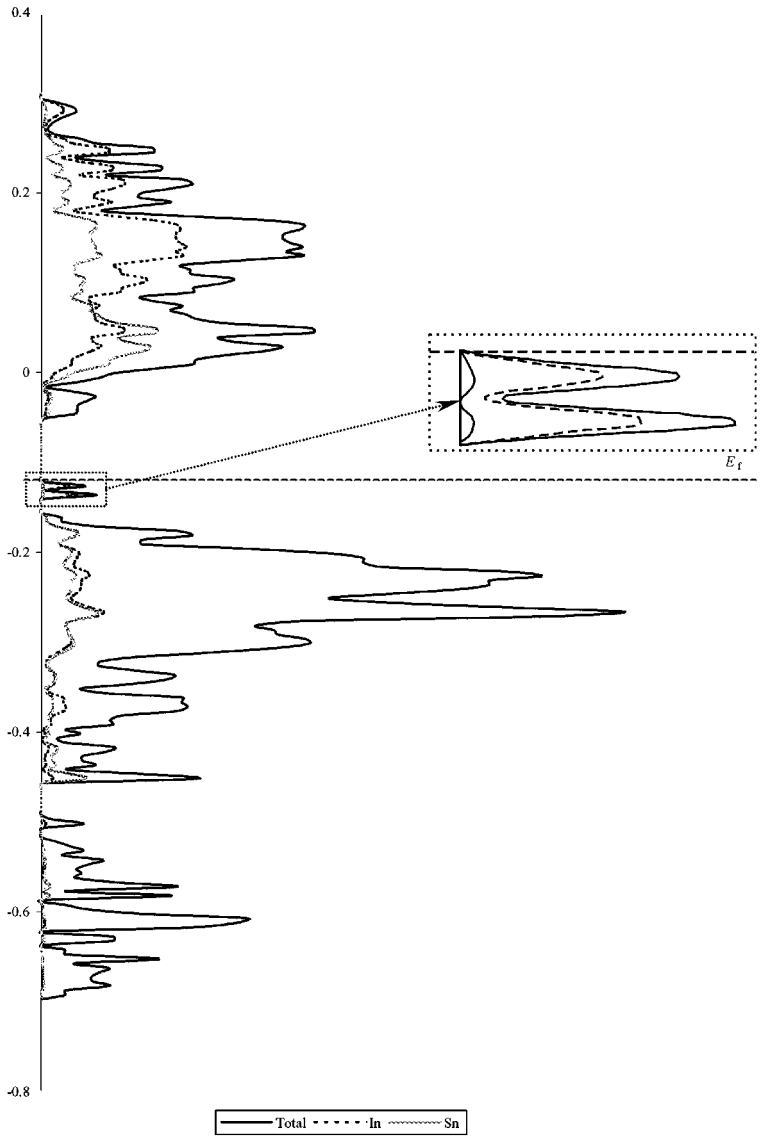

FIG. 5. The DOS for $Sn_{10}In_{14}P_{22}I_8$, hybrid density functional level (B3LYP). $E_F = -0.12$ eV.

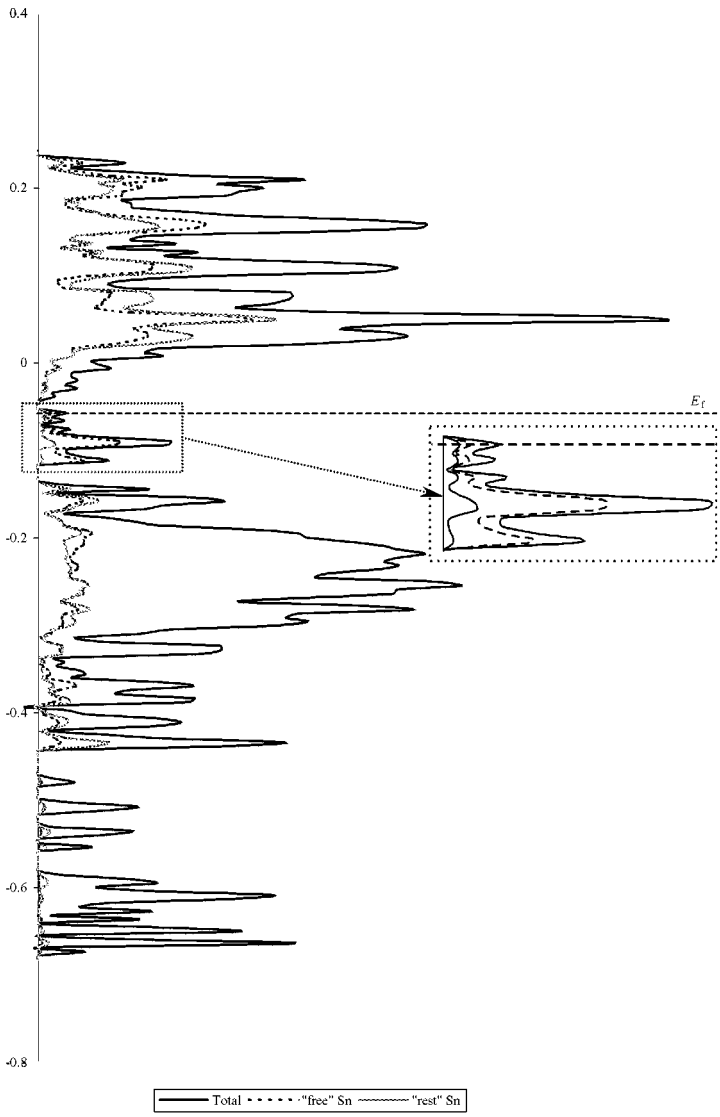

FIG. 6. The DOS for $Sn_{24}P_{19}I_8$, hybrid density functional level (B3LYP). Labeling: "free" Sn, 3 + 3-coordinated tin atoms, "rest" Sn, 4-coordinated tin atoms. $E_F = -0.058$ eV.

The analysis of the DOS curves of $Sn_{10}In_{14}P_{22}I_8$ and $Sn_{24}P_{19}I_8$ reveals two remarkable features of their electronic structures. First, in both cases, the contributions of tin (and indium) and phosphorus are spread over the whole energy spectrum, but all bands just below the Fermi level are formed mainly by the metal orbitals. Accordingly, electronic properties of these compounds are probably associated with the metal substructures. In $Sn_{10}In_{14}P_{22}I_8$ there are two sharp peaks directly below the Fermi level (Fig. 5), which are predominantly indium states. This indicates that the nature of the substituting metal must greatly influence the electronic properties of the tin clathrates.

Second, the states just below the Fermi level in $Sn_{24}P_{19}I_8$ are mainly composed of the 3 + 3-coordinated tin atoms. That has a consequence in the ^{119}Sn Mössbauer spectrum. The above-discussed low quadrupole splitting of a signal assigned to the 3 + 3-coordinated tin atoms may be associated with the electron density reduction on the tin nuclei due to the excitation to the thermally at room temperature accessible conduction band. Figure 6 shows that the bottom of the conducting band is composed of tin and phosphorus orbitals. Consequently, only the Sn–Sn and Sn–P interactions participate in "suppressing" the Sn(II) lone electron pair. That is in contrast with $CsSnBr_3$ (27) and related compounds, where the high-lying *d* orbitals of the halogens serve as the acceptor bands. The Mulliken population analysis of the clathrates' electronic structures shows that only a very weak interaction between the iodines and the host

framework occurs. The iodine atoms carry a high negative charge, up to -0.95 in the case of the iodine atom inside the 24-vertex cage of $Sn_{24}P_{19}I_8$. Therefore, the iodines can be considered as I^- anions preserving electroneutrality, despite the arguments that the guest atoms, in particular Sr in $Sr_8Ga_8Ge_{38}$, are not ionized (13).

Therefore, electric conductivity in the cationic tin clathrates occurs through the framework, not involving the guest atoms, and can be tuned by substitutions. The vacancies in the framework do not produce lone electron pairs, as usually schematized in the frame of the Zintl–Klemm formalism, but rather provoke the formation of delocalized bands in the vicinity of the Fermi level. Finally, the iodines in the 24-vertex cages have large and anisotropic thermal displacement parameters (Fig. 1). They "rattle" inside the voids; such vibrations may reduce thermal conductivity due to resonant scattering of phonons (28). All taken together, this suggests that the cationic tin clathrates deserve investigation with respect to their transport properties as potential thermoelectric materials.

ACKNOWLEDGMENTS

This research is supported by the Russian Foundation for Basic Research, Grant 00-03-32539a, and by INTAS, Contract No. 99-01672.

REFERENCES

1. J. Gallmeier, H. Schäfer, and A. Weiss, *Z. Naturforsch.* **24,** 665 (1969).
2. C. Cros, M. Pouchard, and P. Hagenmüller, *Bull. Soc. Chim. Fr.* **1971,** 379 (1971).
3. Yu. N. Grin′, L. Z. Melekhov, K. A. Chutonov, and S. P. Yatsenko, *Kristallografiya* **32,** 497 (1987).
4. J.-T. Zhao and J. D. Corbett, *Inorg. Chem.* **33,** 5721 (1994).
5. K. W. Allen, *J. Chem. Soc.* 4131 (1959).
6. G. J. Miller, *in* "Chemistry, structure and bonding of Zintl phases and ions" (M. S. Kauzlarich, Ed.), pp. 1–59. VCH, New York, 1996.
7. M. Baitinger, Yu. Grin, and H. G. von Schnering, "Book of Abstracts," VIth European Conference on Solid State Chemistry, Zürich, Sept. 17–20, 1997, PA116.
8. G. K. Ramachandran, P. F. McMillan, J. Dong, and O. F. Sankey, *J. Solid State Chem.* **154,** 626 (2000).
9. G. K. Ramachandran, P. F. McMillan, J. Diefenbacher, J. Gryko, J. Dong, and O. F. Sankey, *Phys. Rev. B* **60,** 12294 (1999).
10. S. Yamanaka, E. Enishi, H. Fukuoka, and M. Yasukawa, *Inorg. Chem.* **39,** 56 (2000).
11. H. G. von Schnering and H. Menke, *Angew. Chem.* **84,** 30 (1972).
12. M. M. Shatruk, K. A. Kovnir, A. V. Shevelkov, I. A. Presniakov, and B. A. Popovkin, *Inorg. Chem.* **38,** 3455 (1999).
13. B. B. Iversen, A. E. C. Palmqvist, D. E. Cox, G. S. Nolas, G. D. Stucky, N. P. Blake, and H. Metiu, *J. Solid State Chem.* **149,** 455 (2000).
14. G. S. Nolas, T. J. R. Weakley, and J. L. Cohn, *Chem. Mater.* **11,** 2470 (1999).
15. G. S. Nolas, J. L. Cohn, G. A. Slack, and S. B. Schujman, *Appl. Phys. Lett.* **73,** 178 (1998).
16. "Handbuch der Präparativen Anorganischen Chemieä" (G. Brauer, Ed.), Ferdinand Enke Verlag, Stuttgart, 1975.
17. G. M. Sheldrick, *in* "Crystallographic Computing 3" (G. M. Sheldrick, C. Kruger, and R. Goddard, Eds.), p. 175. Oxford Univ. Press, Oxford, 1985.
18. G. M. Sheldrick, *in* "Crystallographic Computing 6" (H. D. Flack, L. Parkanyi, and K. Simon, Eds.), p. 111. Oxford Univ. Press, Oxford, 1993.
19. V. R. Saunders, R. Dovesi, C. Roetti, M. Causá, N. M. Harrison, R. Orlando, and C. M. Zicovich-Wilson, "CRYSTAL98 User's Manual". University of Torino, Torino, 1998.
20. P. J. Hay and W. R. Wadt, *J. Chem. Phys.* **82,** 284 (1985).
21. H. G. von Schnering and W. Hönle, *Chem. Rev.* **88,** 243 (1988).
22. C. H. Townes and B. P. Dailey, *J. Chem. Phys.* **17,** 782 (1949).
23. M. M. Shatruk, Dissertation, Moscow State Univ., Moscow, 2000.
24. O. Olofsson, *Acta Chem. Scand.* **24,** 1153 (1970).
25. K. Yamada, T. Matsui, T. Tsuritani, T. Okuda, and S. Ichiba, *Z. Naturforsch. A* **45,** 307 (1990).
26. J. D. Donaldson, R. M. A. Grimsey, and S. J. Clark, *J. Phys.* **40,** 389 (1979).
27. S. J. Clark, C. D. Flint, and J. P. Donaldson, *J. Phys. Chem. Solids* **42,** 133 (1981).
28. J. L. Cohn, G. S. Nolas, V. Fessatidis, T. H. Metcalf, and G. A. Slack, *Phys. Rev. Lett.* **82,** 779 (1999).